Science of the Total Environment 768 (2021) 144659

Contents lists available at ScienceDirect

Science of the Total Environment

journal homepage: www.elsevier.com/locate/scitotenv

Epigenetic effects of silver nanoparticles and ionic silver in *Tetrahymena thermophila*

Yongbo Pan [a,b,c], Senjie Lin [a,b,d], Wenjing Zhang [a,b,c,*]

[a] State Key Laboratory of Marine Environmental Science, Marine Biodiversity and Global Change Research Center, and College of Ocean & Earth Sciences, Xiamen University, Xiamen 361005, China
[b] Xiamen Key Laboratory of Urban Sea Ecological Conservation and Restoration, Xiamen University, Xiamen 361005, China
[c] Fujian Key Laboratory of Coastal Pollution Prevention and Control, Xiamen University, Xiamen 361005, China
[d] Department of Marine Sciences, University of Connecticut, Groton, CT 06340, USA

HIGHLIGHTS

- Ag^+ and Ag NPs are both toxic to *T. thermophila* mainly via causing oxidative stress.
- The toxicity of Ag NPs depends on their physicochemical properties.
- LncRNA-mRNA cascade regulates *T. thermophila*'s response to Ag^+ and Ag NPs exposure.
- *T. thermophila* activated antioxidant response via lncRNA-mRNA co-expression networks.

GRAPHICAL ABSTRACT

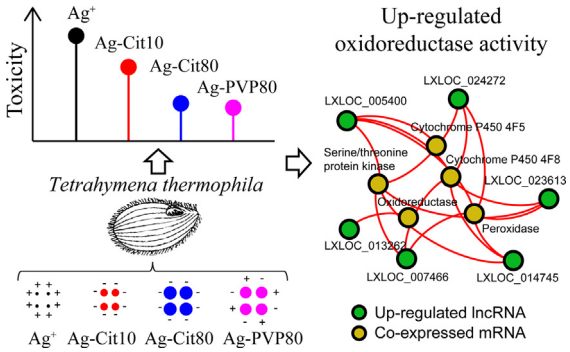

ARTICLE INFO

Article history:
Received 27 October 2020
Received in revised form 8 December 2020
Accepted 18 December 2020
Available online 29 January 2021

Editor: Julian Blasco

Keywords:
Silver nanoparticles
Tetrahymena thermophila
lncRNA
Epigenetic
Co-expression network

ABSTRACT

The widespread use of silver nanoparticles (Ag NPs) has raised substantial health risks, but little is known about the epigenetic toxicity induced by Ag^+ and Ag NPs. This study characterized physiological and lncRNA profiles to explore the toxic effects and epigenetic mechanisms in *Tetrahymena thermophila* on exposure to Ag^+ (in the form of $AgNO_3$) and different Ag NPs for 24 h. The Ag NPs studied varied in size (10 nm and 80 nm) and surface coating (citrate and polyvinylpyrrolidone). We found that both Ag^+ and Ag NPs elicited strong growth-inhibiting effects on *T. thermophila*. The toxicity was mainly caused by high reactive oxygen species (ROS) levels, leading to lipid peroxidation and mitochondrial dysfunction. To combat the oxidative stress, the protist activated an antioxidative response, increasing the activity of glutathione peroxidase and other antioxidants. Notably, 1250 lncRNAs were differentially expressed under Ag^+ or Ag NPs exposure relative to the non-exposure control, which were clustered into 15 expression modules in weighted gene co-expression network analysis. These gene modules exhibited toxicant-specific expression patterns, potentially playing regulatory roles, via their co-expressed mRNAs, to inhibit cell growth, activate cell membrane cation channel, and promote oxidoreductase activity. This research illuminates how post-transcriptional mechanisms of a ciliated protozoan regulate responses to Ag^+ and Ag NPs toxicities.

1. Introduction

Silver nanoparticles (Ag NPs) are one of the largest families of nanomaterials used in the personal care, biomedicine, and food industry due to their excellent antimicrobial activity (Tortella et al., 2020).

* Corresponding author at: State Key Laboratory of Marine Environmental Science, Marine Biodiversity and Global Change Research Center, and College of Ocean & Earth Sciences, Xiamen University, Xiamen 361005, China.
E-mail address: zhangwenjing@xmu.edu.cn (W. Zhang).

https://doi.org/10.1016/j.scitotenv.2020.144659
0048-9697/

Currently, nearly a quarter of nanoproducts contain Ag NPs (Vance et al., 2015), and the annual global production of Ag NPs amounts to 320–420 tons, with projected 800 tons by 2025 (Calderón-Jiménez et al., 2017). Undoubtedly, the extensive and increasing use of Ag NPs would inevitably yield cumulative exposure to human beings and the environment.

Until now, the potential threats of Ag NPs had been shown in a range of organisms, including bacteria, fungi, algae, protozoa, and fish (Bondarenko et al., 2013; Tortella et al., 2020). For example, Lu et al. (2020) demonstrated that both spherical Ag NPs and fibrous silver nanorods could inhibit *Pseudomonas aeruginosa* growth, generate high-level oxidative stress, and cause cell membrane damage. Zhang et al. (2019) found that Ag NPs compromise female embryonic stem cell differentiation. Piersanti et al. (2020) reported that the sublethal concentrations of Ag NPs exposure could induce oxidative stress in *T. thermophila*, causing various gene expression alterations. Several toxicity mechanisms of Ag NPs have been suggested, such as the dissolution of the toxic silver ions (Xiu et al., 2012), generation of reactive oxygen species (ROS) (Wang et al., 2017), and direct disruption of cell membranes (Sekine et al., 2017). Additionally, the physicochemical properties of Ag NPs, such as shape, particle size, the released ions, and the surface coating, influence their toxicity because these properties alter the fate and behaviors of Ag NPs in the test medium (Akter et al., 2018). Numerous studies have attempted to distinguish the toxic effects and molecular mechanisms between Ag^+ and Ag NPs, as well as among different types of Ag NPs (Ivask et al., 2014a; Ivask et al., 2014b; Lu et al., 2020; Yang et al., 2019). For example, the nanoparticles' surface characteristics were the main factor determining the pathways involved in bacterial responses to Ag NPs (Ivask et al., 2014a). The PVP-coding Ag NP has been shown to cause a differentiated transcriptomic profile to Ag NM300K in *Enchytraeus crypticus* (Gomes et al., 2017). Compared to the well characterization of the biological toxicity effects of Ag NP, the epigenetic toxicity of Ag NPs on organisms remains poorly elucidated.

Epigenetic regulations include DNA methylation, histone modification, and noncoding RNA (ncRNA) expression, which controls gene expression in response to internal or external stimuli (Gedda et al., 2019; Yu et al., 2020). ncRNA is a class of functional RNAs that regulate gene expression transcriptionally or post-transcriptionally during development and tumorigenesis (Marchese et al., 2017). Long noncoding RNAs (lncRNAs) are one type of ncRNAs that regulate immune response, cell differentiation, cell cycle, and RNA splicing (Chen et al., 2019). Furthermore, lncRNAs have been suggested to be novel biomarkers of nanotoxicology (Wu et al., 2016; Zhang et al., 2019), but lncRNA expression signatures of response to Ag NPs remain largely unexplored.

In light of the importance of epigenetic processes in the control of gene expression in response to external stimuli, we recently investigated the potential function of microRNA (short ncRNAs) in ciliate *Euplotes vannus* to cope with Ag NP toxic (Pan et al., 2018). However, in that study, only one type of Ag NPs was examined, and the potential differential toxic effects and underlying mechanisms of silver ions and different types of Ag NPs were not explored. In the present study, we used the model species of ciliates *Tetrahymena thermophila* to (i) investigate the epigenetic response of *T. thermophila* to exposure of Ag^+ and three types of Ag NPs, and (ii) address the particle size- or surface coating- specific epigenetic toxicity of Ag NPs. Collectively, our findings will enhance the understanding of how gene post-transcriptional regulatory mechanisms of ciliated protozoa respond to the toxicity induced by Ag^+ and Ag NPs.

2. Materials and methods

2.1. Silver nanomaterials

Three types of Ag NPs, including 10 nm citrate-coated Ag NPs (Ag-Cit10), 80 nm citrate-coated Ag NPs (Ag-Cit80), and 80 nm polyvinylpyrrolidone-coated Ag NPs (Ag-PVP80) were purchased from nanoComposix company (https://nanocomposix.com/). Silver nitrate ($AgNO_3$ > 99%), which was used as an Ag^+ control, was purchased from Sigma-Aldrich (https://www.sigmaaldrich.com/). The basic characteristics of the Ag NPs were provided by nanoComposix and are summarized in Table S1, including diameter, hydrodynamic diameter, zeta potential, and max absorption band. The Ag^+ dissolution rates in the test medium of these NPs were detected by ICP-MS and are summarized in Fig. S1.

2.2. Inhibition assay of Ag^+ and Ag NPs treatments on T. thermophila

The ciliated protozoa *T. thermophila* (strain SB210, provided by Prof. Miao Wei, institute of hydrobiology, Chinese Academy of Sciences) was used as the test organism. Colonial cultures were maintained in the SSP medium in a humidified 28 °C incubator. *T. thermophila* cells were inoculated into a concentration series of Ag^+ and Ag NPs for 24 h as summarized in Table S2. Cell numbers were counted under the microscope with a hemocytometer. Results were analyzed, and the half maxima inhibition rate (IC_{50}) was determined using the probit model of the 'drfit' package in R.

2.3. Determination of the enzyme activity

After the 24 h IC_{50} of the Ag^+ and Ag NPs were determined, *T. thermophila* was exposed to these toxicants' IC_{50} concentration for 24 h, respectively. Then, the cells were harvested and used for detecting the reactive oxygen species (ROS), malondialdehyde (MDA), intracellular ATP, glutathione peroxidase (GPx), and glutathione reductase (Gr). Briefly, DCFH-DA was used to determine the amount of ROS generated in the *T. thermophila*. After DCFH-DA staining, the fluorescence intensity of cells was detected by a flow cytometer in the FL1 channel (BD C6, USA) and Olympus BX51 microscope (Olympus Optical, Tokyo, Japan). MDA was measured using a Lipid Peroxidation MDA Assay Kit. ATP levels were determined using the luciferin-luciferase-based ATP Assay Kit. GPx and Gr were determined using the Cellular Glutathione Peroxidase Assay Kit and Glutathione Reductase Assay Kit, respectively. The total protein of each sample was measured and used for normalizing the enzyme activity. All of the assay kits were purchased from Beyotime Co., China, and the assays were carried out according to the manufacturer's instructions. Details as described in our previous study (Pan et al., 2018).

2.4. RNA isolation and sequencing

We conducted RNA (including lncRNA and mRNA) sequencing for *T. thermophila* collected after Ag^+ and Ag NPs treatment at IC_{50} concentration for 24 h. Total RNA was isolated from *T. thermophila* with the TRIzol reagent (Thermo Scientific), and its concentration was measured using Nanodrop 2000 (Thermo Scientific). The RNA samples were then used for lncRNA sequencing using Illumina HiSeq X-ten with pair-end 150-bp read length. The original lncRNA-seq data have been deposited in the GEO database (GSE157616).

2.5. Bioinformatic analyses

The adaptors and low-quality bases (quality score < 30) were removed from the raw reads. Clean reads were then mapped to *T. thermophila* genome using HISAT (Kim et al., 2015). Next, the transcriptomes were assembled using StringTie (Pertea et al., 2015). The assembled transcripts were then compared to the genome annotation of *T. thermophila* by using Cufflinks (Cuffcompare). LncRNAs were identified from the de novo assemblies with the following steps: (1) tRNA and rRNA transcripts were removed; (2) transcripts less than 200 bp were removed; (3) the transcripts encoding proteins and protein domains were searched against the Pfam databases with cutoff

E-value <0.001 (Finn et al., 2016); (4) transcripts that did not pass the protein-coding-score test using the Coding Potential Calculator (CPC) (Kong et al., 2007), Coding-Non-Coding Index (CNCI) and txCdsPredict software (Sun et al., 2013) were removed. After that, we mapped the clean reads to the *T. thermophila* genome by bowtie 2 (Langmead and Salzberg, 2012), then counted and normalized the expression of mRNA and lncRNA transcripts by RSEM (Li and Dewey, 2011). Differentially expressed genes (DEGs) were evaluated using the DEGseq package (Wang et al., 2010) at the threshold of $|\log_2$ fold change (FC)$| > 1$ and False Discovery Rate (*FDR*) < 0.01.

2.6. lncRNA-mRNA co-expression network

To interrogate the functional role of lncRNA, we first performed WGCNA (Langfelder and Horvath, 2008) to find expression modules that link the differentially expressed mRNAs and lncRNAs, respectively. For each gene module, eigengene was chosen to represent the expression pattern. Further, we conducted lncRNA-mRNA co-expressed network analysis. Each lncRNA module resulting from WGCNA was independently correlated to all mRNA to generate the lncRNA-mRNA correlation pair. As a comparison, all differentially expressed lncRNAs were correlated to all mRNA to generate a total lncRNA-mRNA correlation pair pool. Next, we filtered the result by the threshold of absolute correlation coefficient ≥ 0.8 and *p*-value <0.01. The filtered gene pairs were used to generate the lncRNA-mRNA co-expression network by Gephi 0.9.2, and the mRNA from each co-expression network was used for Gene Ontology (GO) enrichment analysis performed on an R package 'clusterprofiler'.

2.7. RT-qPCR validation

One microgram RNA was firstly subjected to DNA depletion, then reverse-transcribed using the PrimeScrip RT Reagent Kit (TaKaRa). The cDNA products were used for RT-qPCR analyzed with a Fast Start Universal SYBR Green Master (Roche). Gene-specific and GAPDH primers were designed and synthesized from Sangon Biotech (Shanghai) Co., Ltd. (Table S3). The normalized RT-qPCR results was performed using the $2^{-\Delta\Delta Ct}$ method with GAPDH as the reference gene.

2.8. Statistical analyses

Data from three biological replicates were averaged to yield mean ± SD. One-way ANOVA with LDS's test was used to compare data between groups, and $p < 0.05$ was accepted as statistical significance.

3. Results

3.1. Cell growth of T. thermophila inhibited by Ag+ and Ag NPs

Based on cell counts were done after 24 h exposure, both Ag^+ and Ag NPs led to a dose-dependent inhibition in *T. thermophila* growth (Fig. 1 A). Based on the inhibition rate, the 24 h IC_{50} values were calculated to be 0.86 ± 0.06, 1.64 ± 0.14, 2.68 ± 0.1 and 2.93 ± 0.08 mg/L for Ag^+, Ag-Cit10, Ag-Cit80 and Ag-PVP80, respectively (Fig. 1 B). Ag^+ was more toxic than Ag NPs ($p < 0.05$), and small-sized Ag NPs were more toxic than large-sized counterparts ($p < 0.05$), while the toxicity of Ag NP with Cit-coating was slightly higher than that with PVP-coating but with no statistical significance ($p > 0.05$, Fig. 1 B).

3.2. Ag+ and Ag NPs induced oxidative stress to T. thermophila

In order to evaluate the toxicity mechanisms of Ag^+ and Ag NPs in *T. thermophila*, we conducted an experiment using the IC_{50} concentration of Ag^+ and Ag NPs to treat the *T. thermophila* for 24 h, respectively. From microscopic observations, we found that the Ag^+ treatment caused *T. thermophila* cilia shedding, increased cell membrane permeability and decreased swimming ability, while Ag NPs treatment caused *T. thermophila* cell deformation and cell membrane enrichment with black spots, but with cilia kept intact (Fig. 2). These results were indicative that the Ag NPs had internalized the cells. Further, we measured ROS content in *T. thermophila* based on DCF fluorescence and found that all of the four toxicants generated a high level of ROS after 24 h treatment and were significantly higher than the control group (Fig. 2). We next evaluated the cellular MDA content, which indicates the degree of lipid peroxidation. Results showed that both Ag^+ and Ag NPs caused significant lipid peroxidation of the cell membrane (Fig. 3A). Interestingly, the ROS generation and MDA content showed a similar increasing trend, suggesting that the oxidative stress induced lipid peroxidation. Additionally, the intracellular ATP level was significantly decreased under 24 h Ag^+ and Ag NPs treatment (Fig. 3B), indicating that these toxicants likely caused the mitochondrial dysfunction of *T. thermophila*. These results indicated that oxidative stress was one of the main mechanisms that Ag NPs and Ag^+ were toxic to *T. thermophila*. To strengthen this idea, we further evaluated the GPx and Gr activity after Ag^+ and Ag NPs exposure. Results showed that GPx was significantly increased while Gr was significantly decreased (Fig. 3C and D), consistent with the increasing trend of ROS because higher activities of GPx or lower activities of Gr indicate higher levels of ROS.

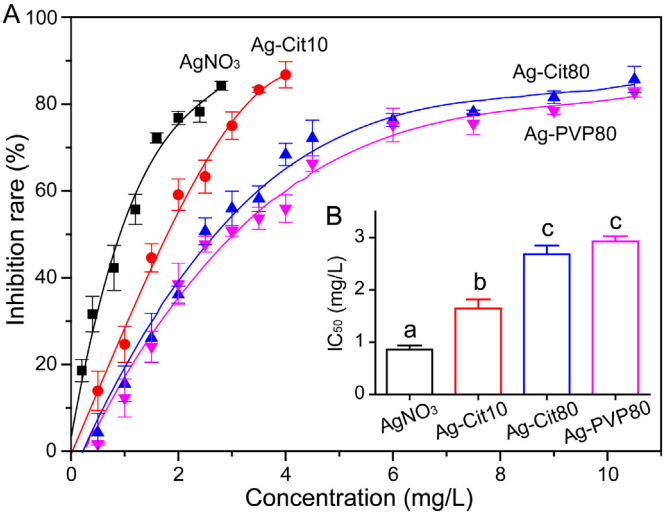

Fig. 1. Growth inhibiting effects of Ag^+ and Ag NPs to *Tetrahymena thermophila*. (A) Growth inhibition rate of *T. thermophila* exposure to Ag^+ (in the form of $AgNO_3$), Ag-Cit10, Ag-Cit80 and Ag-PVP80 at different concentrations for 24 h. (B) 24_h IC_{50} values of the four toxicants on *T. thermophila*. Error bars indicate ± standard deviations of the biological triplicates. Different letters on top of bars indicate significant difference ($p < 0.05$).

3.3. Global lncRNA and mRNA responses under Ag+ and Ag NPs exposure

To evaluate the molecular response of *T. thermophila* under Ag^+ and Ag NPs exposure, we performed a genome-wide lncRNA sequencing. Approximately 1838 million reads were obtained from the 15 sequencing libraries (Table S4). Both Q30 values and GC contents suggested the accuracy and reliability of the lncRNA-seq data (Table S4). De novo transcript assembly yielded a total of 29,879 transcripts, with 6478 lncRNAs and 23,401 mRNAs. We found that the mean length of lncRNA transcripts (1573 bp) was shorter than mRNA (1909 bp) (Fig. S2), and the global expression of lncRNA was significantly lower than mRNA in control and each treatment group (Fig. 4A). Principal component analysis (PCA) revealed that the biological replicate samples of each treatment represent a distinct cluster, except for Ag-Cit10 and Ag-Cit80 that based on lncRNA expression (Fig. 4B).

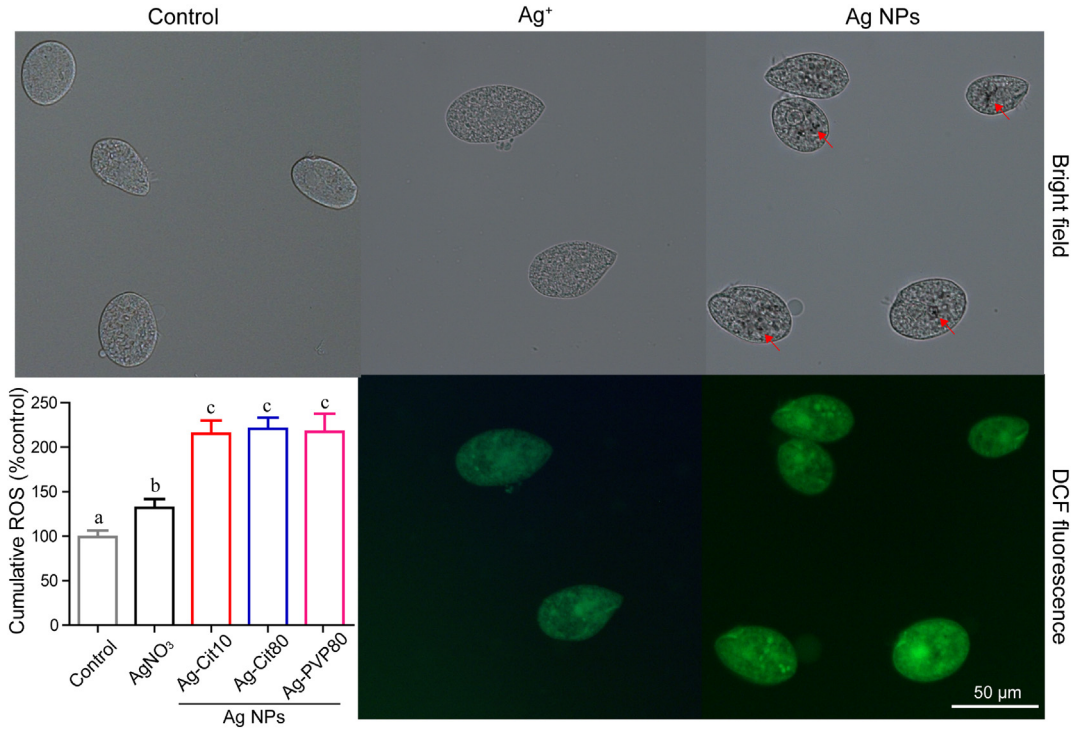

Fig. 2. Representative graphs showing the accumulation of ROS in *T. thermophila* after Ag^{+} and different types of Ag NPs exposure for 24 h. Red arrows indicate Ag NPs enriched in the cells. Graph showing the relative fluorescence intensity in the four treatment groups compared to the control group. Error bars indicate ± standard deviations of biological triplicates, and different letters on top of bars indicate significant difference ($p < 0.05$). (For interpretation of the references to colour in this figure legend, the reader is referred to the web version of this article.)

By using a cutoff $|\log_2(FC)| > 1$ and $FDR < 0.01$, we totally identified 1250 differentially expressed lncRNA (DE lncRNA) and 2909 differentially expressed mRNA (DE mRNA) (Fig. 4C). The number of DE lncRNA was similar in different treatment groups, with 430, 431, 487, and 590 were identified in Ag^{+}, Ag-Cit10, Ag-Cit80, and Ag-PVP80, respectively, while the number of DE mRNA was varied,

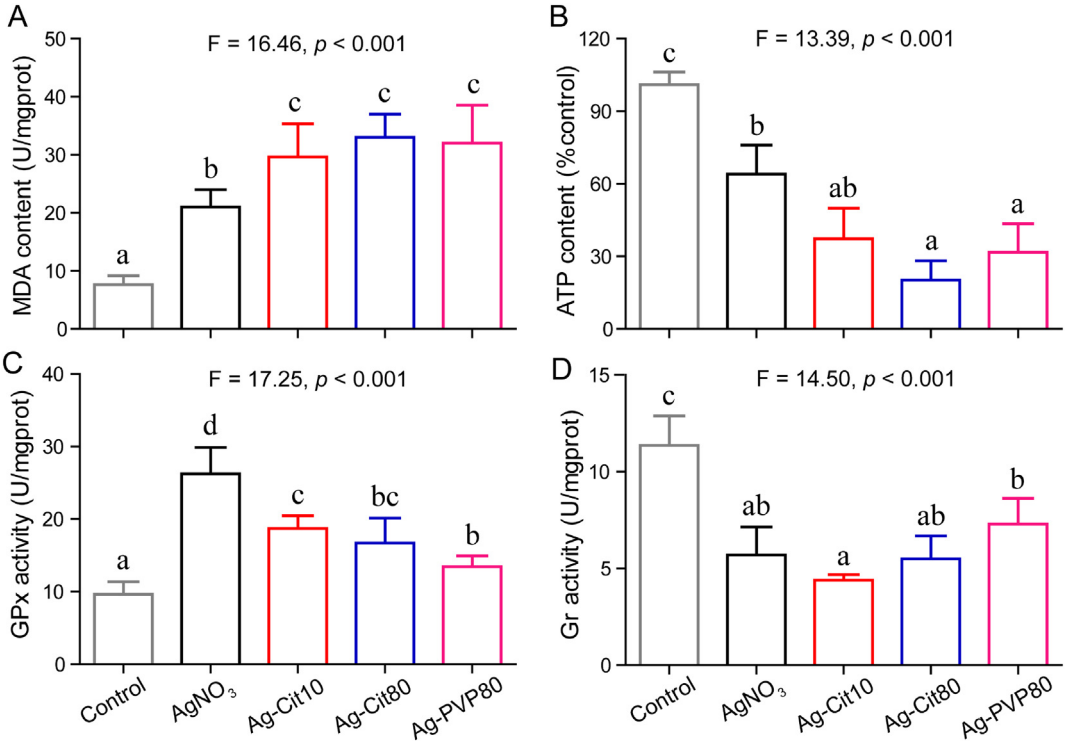

Fig. 3. Biochemical activities of *T. thermophila* after Ag^{+} and Ag NPs exposure for 24 h. (A) Malondialdehyde (MDA) contents, (B) ATP levels, (C) Glutathione peroxidase (GPx), (D) Glutathione reductase (Gr). Error bars indicate ± standard deviations of biological triplicates. Different letters on top of bars indicate significant difference ($p < 0.05$).

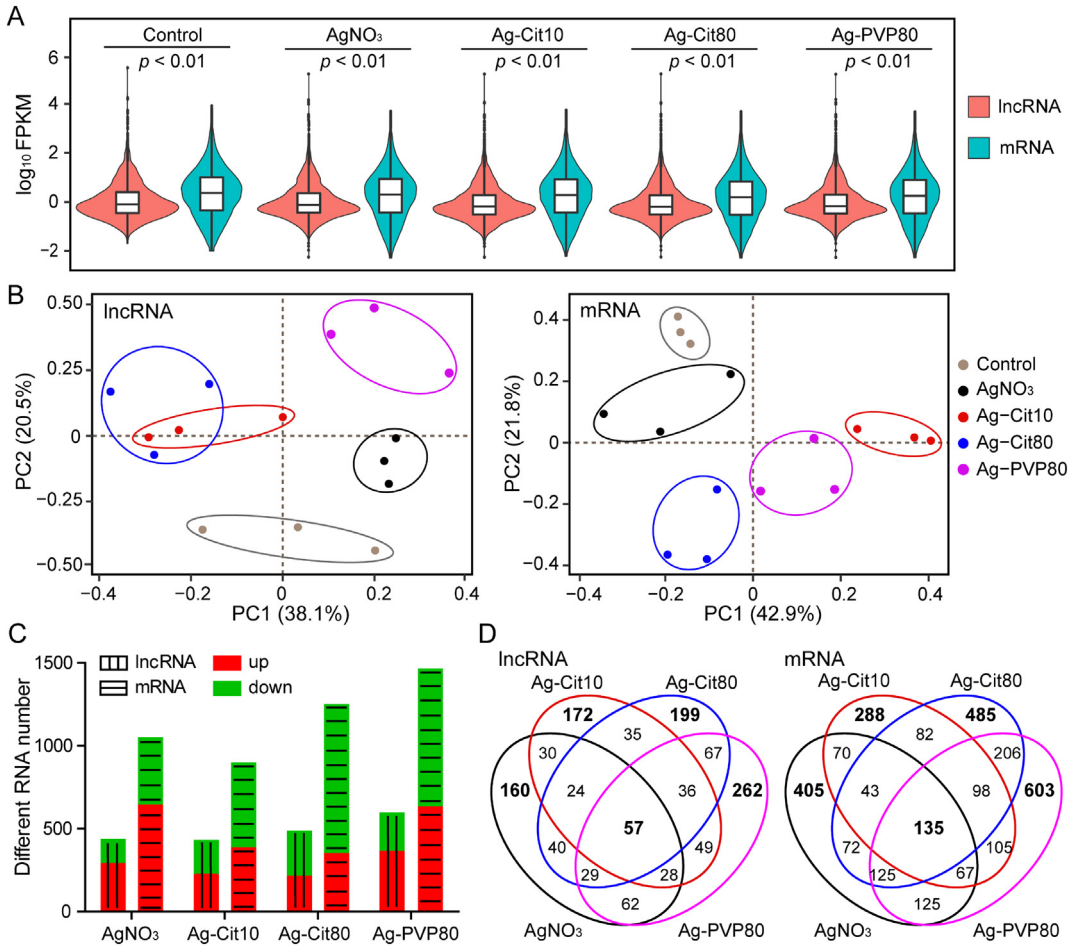

Fig. 4. The discrete expression patterns of lncRNAs and mRNAs. (A) The lncRNA and mRNA expression levels in different treatment groups. (B) Principal component analysis (PCA) of the 15 samples based on normalized lncRNAs and mRNAs expression level. Each dot represents one sample, samples are grouped in circle by treatments. (C) Histogram showing the number of differentially expressed lncRNA and mRNA in each comparison group of treatments relative to the control. (D) Venn diagram showing the number of differentially expressed lncRNA and mRNA for the four treatment groups relative to the control.

as 1042, 888, 1246, and 1464 were identified in Ag^+, Ag-Cit10, Ag-Cit80, and Ag-PVP80, respectively (Table 1). Additionally, we found that 76.43% ~ 91.87% of the DEGs exhibited low expression (define as transcripts with FPKM ≤1) (Table 1), while the low-expression genes in the whole transcripts ranged from 37.63% to 44.56% (Fig. S3), suggesting that the low-expression genes of *T. thermophila* may play an important role in responding to the stress induced by Ag^+ and Ag NPs. Among the DEGs, only 57 DE lncRNAs and 135 DE mRNAs were consistently differentially expressed in all treatment groups, while up to 160, 172, 199, and 262 DE lncRNAs, and up to 405, 288, 485, and 603 DE mRNAs were uniquely differentially expressed in Ag^+, Ag-Cit10, Ag-Cit80, and Ag-PVP80 treatment group, respectively (Fig. 4D), implying that these toxicants affected *T. thermophila* through different toxicological mechanisms.

To further validate the high-throughput sequencing data, we selected five lncRNAs and five mRNAs involved in key biological functions or showed differential expression patterns between treatment and control for RT-qPCR analysis. LncRNA-seq and RT-qPCR results exhibited a similar expression profile (Fig. S4) and a strong spearman correlation ($r = 0.927$, $p < 0.001$) (Fig. S5), indicating the reliability of the lncRNA-seq data.

3.4. Specific-regulation of lncRNAs and mRNAs in Ag+ and Ag NPs induced toxicity

In order to evaluate the expression patterns of the differentially expressed lncRNA and mRNA (1250 DE lncRNAs and 2909 DE mRNAs), we performed WGCNA analysis. Totally 15 lncRNA

Table 1
Statistics of the differentially expressed genes.

	$AgNO_3$		Ag-Cit10		Ag-Cit80		Ag-PVP80	
	lncRNA	mRNA	lncRNA	mRNA	lncRNA	mRNA	lncRNA	mRNA
Total gene	430	1042	431	888	487	1246	590	1464
Up regulated	288	640	232	375	211	346	356	628
Down regulated	142	402	199	513	276	900	234	836
Mean FPKM ≤ 1	391	848	396	785	428	984	514	1119
Mean FPKM 1–10	36	171	34	92	56	212	68	280
Mean FPKM ≥ 10	3	23	1	11	3	50	8	65

transcriptional modules (Fig. 5A) and 19 main mRNA transcriptional modules were identified (Fig. S6), and each of these modules represented a characteristic expression pattern. We next analyzed these modules by heat map graphing and eigengene value graphing. After that, we defined the spatial expression modules of lncRNA or mRNA, which was characterized by remarkably higher expression in a distinct treatment group but less remarkable in others (Figs. 5B, S6B, and Table S5). Three lncRNA modules, LM2 (with 139 lncRNAs), LM10 (with 63 lncRNAs) and LM11 (with 60 lncRNAs) exhibited remarkably higher expression in the Ag^+ treatment group. Similarly, three modules were remarkably more highly expressed in the Ag-Cit10 treatment group (module LM7 with 71 lncRNAs, LM12 with 59 lncRNAs, and LM14 with 51 lncRNAs), Ag-Cit80 treatment group (module LM6 with 76 lncRNAs, LM13 with 55 lncRNAs, and LM15 with 38 lncRNAs), and Ag-PVP80 treatment group (modules LM1 with 176 lncRNAs, LM5 with 81 lncRNAs, and LM8 with 69 lncRNAs), while modules LM3 (with 121 lncRNAs), LM4 (with 91 lncRNAs), LM9 (with 65 lncRNAs) exhibited remarkably higher expression in the control group. These results indicated that *T. thermophila* performed specific regulation of lncRNAs expression in response to Ag^+ and Ag NPs induced toxicity. Similarly, the expression of mRNAs also displayed specific regulation under Ag^+ and Ag NPs exposure (Fig. S6 and Table S5). Further, the gene expression relationship between the lncRNA and mRNA modules were evaluated. Several co-expression genes were detected, including exclusive pairs (e.g. LM6-MM12 and LM7-MM7) and multi-pairs (e.g. LM1-MM9 and LM1-M11, LM3-MM1 and LM3-MM4) (Fig. S7).

3.5. The function of lncRNA was associated with mRNA in response to Ag+ and Ag NPs induced toxicity

To unveil the potential function of lncRNAs, we conducted a Pearson correlation analysis between 1250 DE lncRNAs and 23,401 mRNAs based on their expression in all lncRNA-seq samples. After filtering with $|r| \geq 0.8$ and $p < 0.01$, a total of 8273 strong co-expression pairs were detected (Table S7). Interestingly, most of the co-expression pairs (99.40%) were positively related. Similarly, when the correlation analyses between lncRNA and mRNA, lncRNA and lncRNA, or mRNA and mRNA were conducted, the percentage of positively co-expression pairs was as high as 89.33%, 94.18%, and 74.28%, respectively (Table S7), suggesting that most of the lncRNAs were gene-promoting in *T. thermophila* under Ag^+ and Ag NPs exposure.

To visually demonstrate the relationship between the DE lncRNAs and mRNAs, a lncRNA-mRNA co-expressed network was constructed using Gephi. The constructed network contains 2152 nodes (genes) and 8273 edges (co-expression pairs) (Fig. 6A). The network obtained have shown scale-free characteristics (power-law: $R^2 = 0.89$, Fig. S8), indicating that the network structure was non-random. In the entire co-expressed network, lncRNAs accounted for 13.99%, while mRNAs accounted for 86.01%. Among the mRNAs, 13.34% exhibited differential expression (Fig. 6A). Interestingly, the whole network was clearly parsed into 15 major modules (sub-networks), and each sub-network contained different nodes and edges, and these sub-networks accounted for 73.78% of the whole network (Fig. 6B). Importantly, the 15 sub-networks corresponded to the 15 lncRNA modules associated with mRNAs networks (Fig. 6C). The number of nodes in these 15 co-expressed networks ranged from 79 to 278, among which 19% to 38% were differentially expressed, while the number of edges varied from 243 to 1350 (Table S6). We noticed that some lncRNAs had a high degree (the number of a gene associated with other genes); therefore, these lncRNAs were considered key nodes of the network (Fig. 6C). For example, the highest degree up to 99 occurred in module M2, indicating that a lncRNA was associated with up to 99 mRNAs (Fig. 6C and Table S6).

By combining the toxicant-specific expression patterns of lncRNA modules (Fig. 5), we further explored the function of each lncRNA module based on the co-expressed mRNA. GO enrichment analysis showed that the co-expressed network M3, which was remarkably more highly expressed in the control group compared to treatment groups, was significantly enriched in growth-related process (such as cyclic nucleotide biosynthetic process, nucleotide biosynthetic process, and purine nucleotide biosynthetic process) (Fig. 7). These results were consistent with growth inhibition in *T. thermophila* by Ag^+ and Ag NPs (Fig. 1).

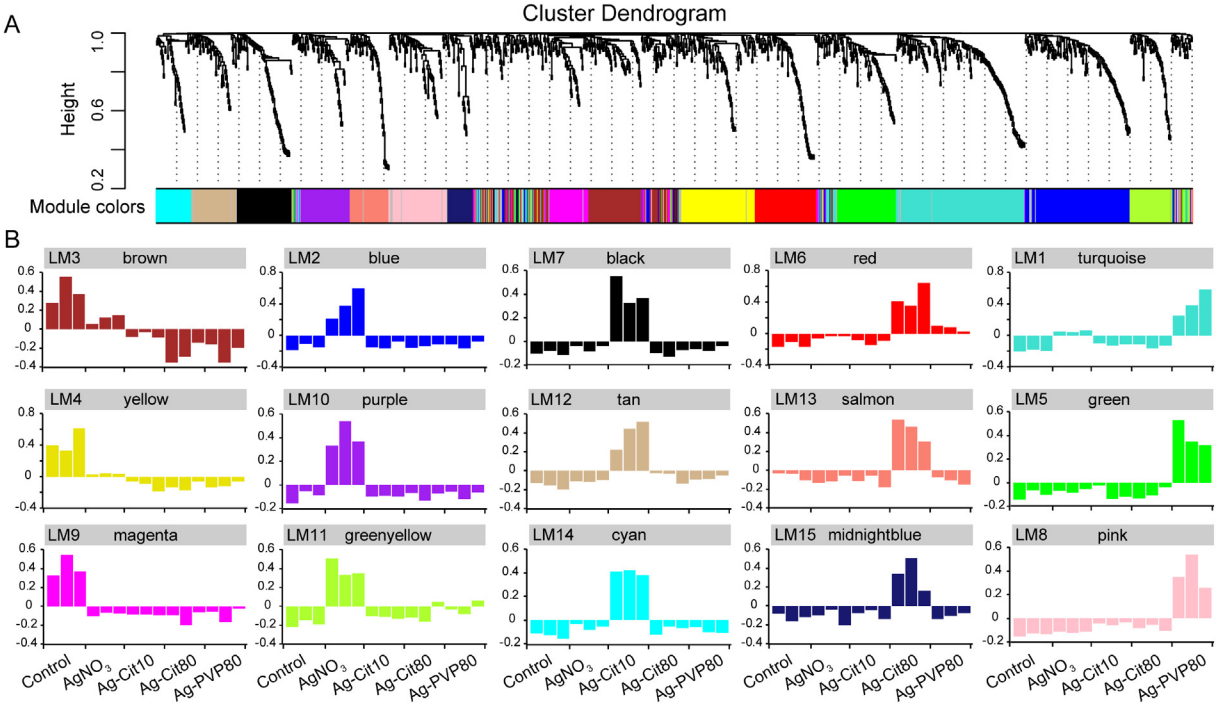

Fig. 5. The discrete expression modules of lncRNA expression by the WGCNA analysis. (A) Differentially expressed lncRNAs were cluster by WGCNA. Different modules generated by WGCNA were labeled with different colors. (B) Eigengene bar plot of the toxicant-specific modules of lncRNAs.

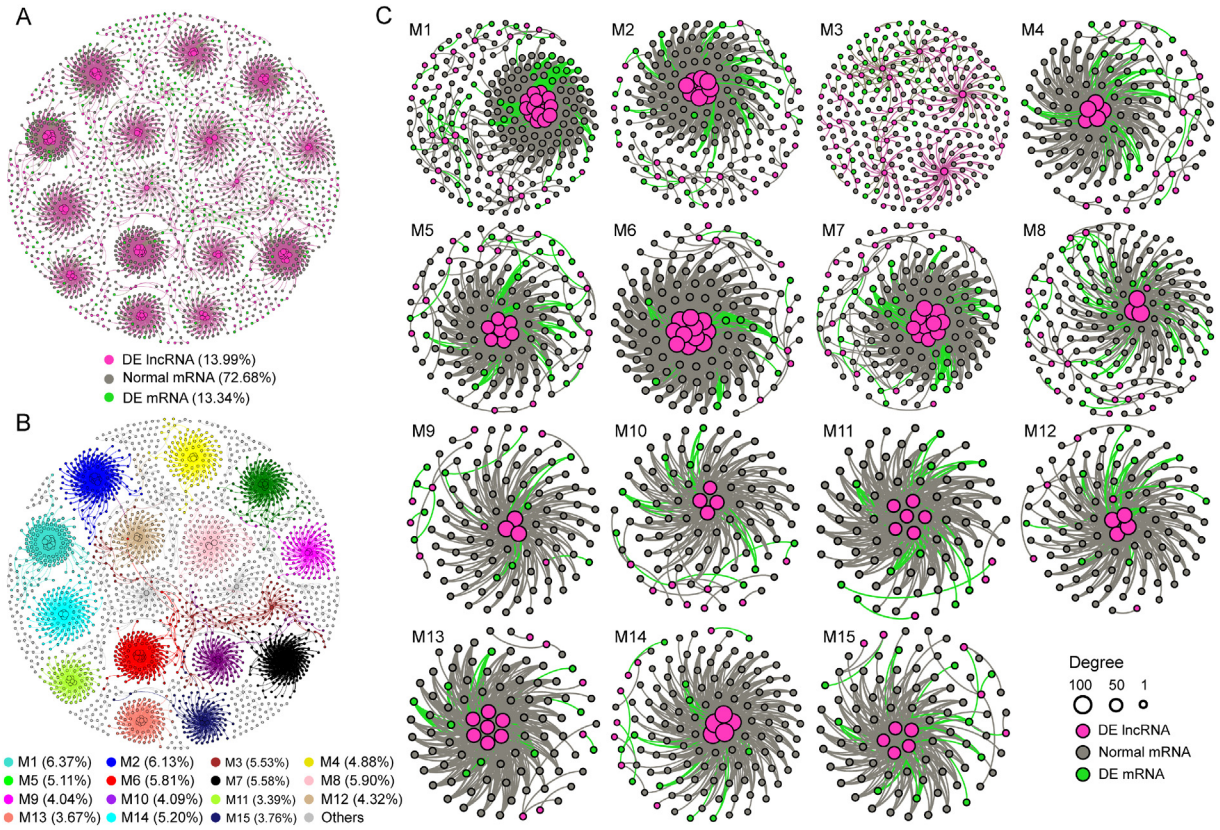

Fig. 6. The panoramic of the lncRNA and mRNA co-expression networks. (A) co-expression networks of DE lncRNAs and mRNAs based on their expression in 15 lncRNA-seq samples. (B) co-expression of DE lncRNAs and mRNAs network colored by modularity class. (C) The fifteen lncRNA modules clustered by WGCNA and their associated mRNAs based on correlation analysis. Each circle represents a gene, the size of the circle represents of the degree to which a gene interacts with others, or the number of genes that this gene is associated with. In (A) and (C), the pink circles represent differentially expressed lncRNA, grey circles represent normal expressed mRNA, green circles represent differentially expressed mRNA. (For interpretation of the references to colour in this figure legend, the reader is referred to the web version of this article.)

Additionally, the co-expressed network M2, which exhibited remarkably higher expression in the $AgNO_3$ treatment group, was significantly enriched in channel-related function (such as ion gated channel activity, voltage-gated ion channel activity, and potassium channel activity) (Fig. 7), indicating that Ag^+ internalized the cells via the transmembrane transport. Interestingly, several co-expressed networks were significantly enriched in enzymatic activities such as peptidase activity and oxidoreductase activity (Fig. 7). These co-expressed networks included M5, M7, M8, M10, M12, M14, and M15, which were remarkably up-regulated in treatment groups, suggesting that the exposure of Ag^+ and Ag NPs had stimuli the enzyme activity which may contribute to detoxification.

4. Discussion

4.1. Varied toxic effects of Ag NPs and Ag+ to T. thermophila

The physical and chemical characteristics of Ag NPs are known to have direct impacts on their biological toxicity (Akter et al., 2018). In recent years, there have been many studies that attempted to characterize the distinction in toxic effects and mechanisms between different types of Ag NPs (Ivask et al., 2014a; Nallanthighal et al., 2020; Silva et al., 2014). In our study, we found different toxic effects between different types of Ag NPs and between Ag NPs and Ag^+ to *T. thermophila*. Firstly, our study demonstrated that Ag NPs with small-sized particles (10 nm) were more toxic than large-sized particles (80 nm, $p < 0.01$). A previous study has suggested that the Ag NPs with small-sized has a higher percentage of surface area compared to the larger one, which makes it release a higher proportion of Ag^+ (Fig. S1), and is easier to enter the cell, thus making it more toxic (Ivask et al., 2014b). Secondly, we found that the Ag NPs coating with citrate or polyvinylpyrrolidone had no significant difference in their toxicity ($p > 0.05$). Citrate and polyvinylpyrrolidone are the most frequently used coating materials to stabilize Ag NPs (Huynh and Chen, 2011). Polyvinylpyrrolidone confers electrostatic and steric stabilization to Ag NPs, whereas citrate only provides electrostatic stabilization, but both types of coating give negative charges (Nallanthighal et al., 2020). Studies have shown that the citrate- and polyvinylpyrrolidone- coated Ag NPs have similar protein absorption ability, protein corona composition, and silver ion release rate (Tejamaya et al., 2012; Pang et al., 2016), which explain their similar toxicity for *T. thermophila*. Thirdly, we found that the Ag^+ was more toxic than any type of Ag NPs as it had lower IC_{50} values (Fig. 1B, $p < 0.01$). A previous study has argued that dissolution of Ag^+ was the primary mechanism of the toxicity for Ag NPs and that particle-specific activity was negligible (Xiu et al., 2012). However, based on the Ag^+ dissolution rate of the Ag NPs on SPP medium (Fig. S1), the release of Ag^+ was calculated to be 0.18 ± 0.01, 0.17 ± 0.01, and 0.22 ± 0.01 mg/L for Ag-Cit10, Ag-Cit80 and Ag-PVP80 under IC_{50} concentration, respectively, all of these were much lower than the IC_{50} concentration of Ag^+ (0.86 ± 0.06 mg/L, $AgNO_3$ treatment group), indicating that the toxicity of Ag NPs was multifactorial, where surface coatings, particle size, and Ag^+ dissolution rate could all be important as our previous study suggested (Pan et al., 2018). Overall, we demonstrate that the toxicity of Ag NPs for *T. thermophila* is highly dependent on their physicochemical properties, and the order of toxicity is: Ag^+ > Ag-Cit10 > Ag-Cit80 > Ag-PVP80.

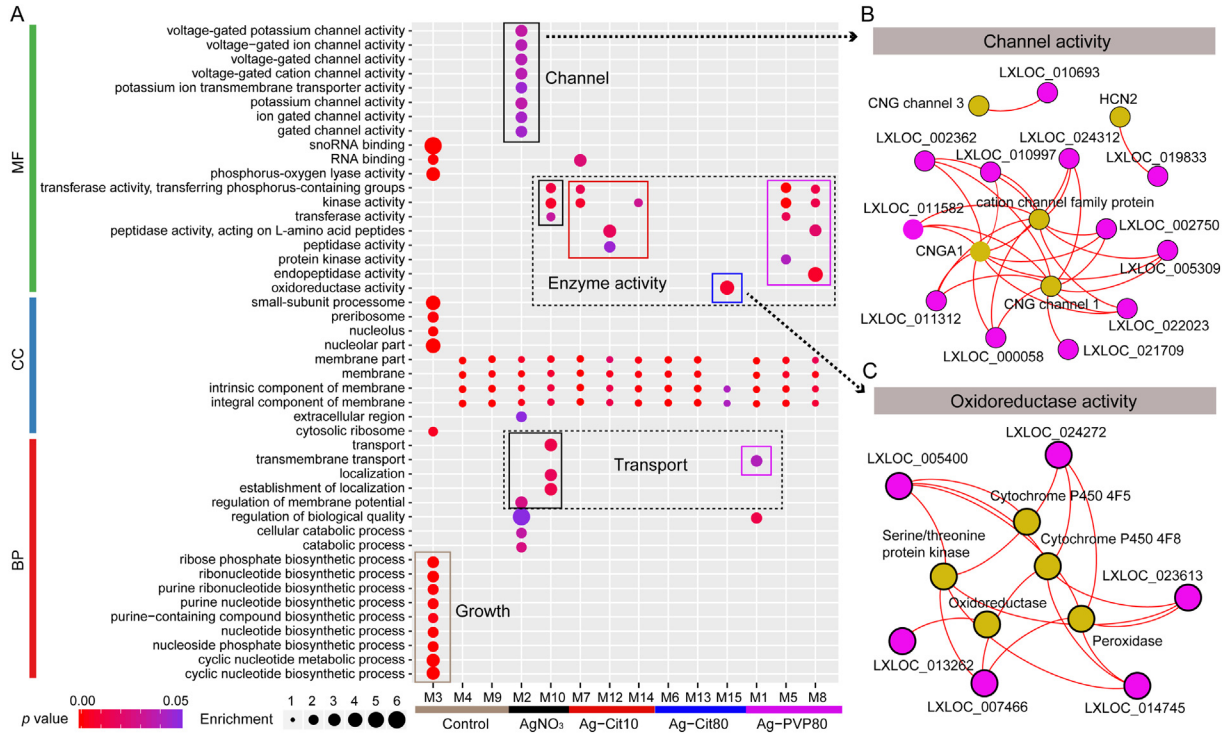

Fig. 7. Gene Ontology analysis of the 15 lncRNA-mRNA co-expression networks. (A) The networks of M3/4/9, M2/10, M7/12/14, M6/13/15 and M1/5/8 were remarkably more highly expressed in control, Ag^+, Ag-Cit10, Ag-Cit80 and Ag-PVP80 group, respectively. The rectangles mark the groups of similar functional GO terms. The co-expression of lncRNA and mRNA in GO terms of Channel activity (B) and Oxidoreductase activity (C). Pink circles represent up-regulated lncRNA, and yellow circles represent Co-expressed mRNA. CNGA1: cGMP-gated cation channel alpha-1; HCN2: Sodium hyperpolarization-activated cyclic nucleotide-gated channel 2; CNG channel 1/3: Cyclic nucleotide-gated cation channel 1/3. (For interpretation of the references to colour in this figure legend, the reader is referred to the web version of this article.)

4.2. Changes in antioxidative activity of T. thermophila in response to Ag NPs and Ag^+ stress

It has been suggested that ROS production plays a significant role in Ag NPs induced toxicity (Flores-Lopez et al., 2019). In our study, we observed that both Ag^+ and Ag NPs induced a high level of ROS in *T. thermophila* after 24 h treatment (Fig. 2). The ROS contents between Ag NPs groups were similar, but all of them were significantly higher than the Ag^+ group (Fig. 2). It has been suggested that Ag NPs may induce mitochondrial damage, which results in ROS generation (Flores-Lopez et al., 2019). Additionally, it has been speculated that the particle surface reactions could generate ROS (Abdal Dayem et al., 2017). On the other hand, Ag^+ can cause protein misfolding and damage as it binds to the thiol group of target proteins or inhibiting ATP synthesis as it replaces Cu^+ in key proteins in ATP synthesis (Pillai et al., 2014). The different toxicity routes may explain the differences in ROS generation between Ag^+ and Ag NPs.

ROS is necessary for cell function; however, ROS will increase under internal or external stimuli, and oxidative stress would occur when the ROS generation and their degradation by the antioxidants defense system are imbalanced (Flores-Lopez et al., 2019). Overproduction of ROS can cause cell damage and apoptosis. These severe effects have been observed in many organisms, such as bacterial (Lu et al., 2020), Zebrafish (Abramenko et al., 2018), and *Caenorhabditis elegans* (Yang et al., 2012). In the present study, we found that both Ag^+ and Ag NPs caused lipid peroxidation, apparently leading to mitochondria dysfunction, suggesting that oxidative stress was one of the primary mechanisms that Ag^+ and Ag NPs were toxic to *T. thermophila*. A similar phenomenon was also observed in a previous study of ours, which focused on the toxic of Ag NP to ciliate *Euplotes vannus* (Pan et al., 2018).

The level and action of harmful ROS in cells were controlled by several protein/enzymatic defense mechanisms such as glutathione (GSH), Gr, and GPx (Ulm et al., 2015). GPx uses GSH to reduce hydrogen peroxide and lipid hydroperoxides, while Gr catalyzes the reduction of glutathione disulfide (GSSG) to the sulfhydryl form GSH (Deponte, 2013). In our study, the GPx activity was upregulated, whereas the Gr activity was downregulated under the Ag^+ and Ag NPs stress (Fig. 3C and D), indicating the constant consumption of GSH for cell detoxification. Besides eliminating ROS, part of the GSH's function may be binding to Ag ions to facilitate its isolation and elimination via the lysosome system, as suggested in Cu ions (Ferro et al., 2015). However, GSH can be biosynthesized ex-novo, thanks to γ-glutamyl cysteine ligase and glutathione synthetase, and which can be induced by metals (Franchi et al., 2012). Therefore, is it possible that the total GSH levels remain at least constant, or even increased, which needs to be further determined. Furthermore, other antioxidant enzymes such as superoxide dismutase (SOD) and peroxiredoxin (Prdx) also contributed to metal detoxification in *T. thermophila* (Ferro et al., 2015; Al-Asadi et al., 2019).

4.3. Response of lncRNA and mRNA under Ag+ and Ag NPs stress

Using a systems biology approach, we examined the global mRNA and lncRNA expression profiles under Ag^+ and Ag NPs exposure in *T. thermophila*. Totally, we identified 6478 lncRNA transcripts, all of which are novel lncRNAs, supporting the idea that the conservation of lncRNA was low between different organisms (Hezroni et al., 2015). The expression of lncRNA was significantly lower than mRNA but fluctuated more widely (Fig. 4A), indicating that the expression of lncRNA was less conservative than mRNA (Liu et al., 2017), consistent with the role of lncRNA as regulators. We identified multiple DEGs in different treatment groups, but the number of DEGs in the Ag-PVP80 group was highest, which is consistent with a recent study which showed that the number of DEGs induced by PVP-coating Ag NP was more than twice higher than Cit-coating Ag NP in mice (Nallanthighal et al.,

2020). These results indicated that the stabilizing agents of Ag NPs strongly influence *T. thermophila* transcriptional responses.

It has been suggested that the expression patterns of lncRNAs are tissue- and stage-specific, consistent with their diverse functional roles (Gloss and Dinger, 2016; Liu et al., 2017). However, until now, the expression patterns of lncRNA in organisms under Ag NPs stress has not been explored. Based on the result of WGCNA, we observed that the lncRNAs had toxicant-specific expression patterns (Fig. 5), demonstrating that the expression of lncRNAs will be specifically high or low under specific toxicant exposure. Therefore, it can be speculated that *T. thermophila* will perform different biological responses under different stress conditions. To verify this postulation, we analyzed the co-expression network of lncRNA and mRNA. The co-expressed lncRNA and mRNA genes often control similar functions (Luo et al., 2017; Nayak et al., 2009), which allows us to explore the functions of lncRNA based on the co-expression of mRNA. We generated a total of 15 lncRNA-mRNA co-expression networks (Fig. 6), and found these networks performed various functions (Fig. 7). Firstly, network M3 is associated with the growth-related process, and the expression of its genes was inhibited under Ag^+ and Ag NPs stress, consistent with the growth-inhibiting nature of Ag^+ and Ag NPs on *T. thermophila*. Secondly, network M2 is associated with ion channel function, and the expression of its genes was promoted under Ag^+ exposure, suggesting that Ag^+ is internalized into the cells via the ion channel of the cell membrane. In this network, five mRNAs (including CNGA1, HCN2, CNG channel 1/3, and a cation channel family protein) were associated with 12 lncRNAs that seem to play an important role in cell membrane cation channel activation (Fig. 7B). This is consistent with the phenomenon that *T. thermophila* cells membrane permeability increased after Ag^+ treatment (Fig. 2). Also, previous studies had verified that the ion channel of cell membrane are involved in Ag^+ uptake into the cells (Solioz and Odermatt, 1995). Thirdly, several networks were significantly enriched in antioxidant enzymes (Fig. 7), suggesting that these networks may contribute to enzymatic elimination of the ROS induced by Ag^+ and Ag NPs. For example, in the co-expression network M15, five mRNAs (including Cytochrome P450 4F5/4F8, Serine/threonine protein kinase, Oxidoreductase, and Peroxidase) associated with six lncRNAs were significantly enriched in the oxidoreductase activity (Fig. 7C). This is supported by the corresponding increase of GPx enzyme activities (Fig. 3C and D), indicating that lncRNAs were involved in regulating the cell detoxification process. Although our data did not significantly enrich any endocytosis-related processes, Ag NPs internalization into the cells was observed under the microscope (Fig. 2). Previous studies have found that Ag NPs can be adsorbed on the cell membranes of *E. coli* (Ivask et al., 2014a) and *T. thermophila* (Mortimer et al., 2014), which also can explain the phenomenon overserved in this study.

The predicted lncRNA function should be verified by further experiments, such as gene silencing, overexpression, and knockout. However, only a few lncRNAs have been functionally verified under Ag NPs exposure, and such research has mainly focused on mammalian cells. For example, the lncRNA *ODRUL* has been proven to regulate the PI4K-AKT/JNK signaling pathway, which negatively regulates the expression of *Bcl-2*, thereby accelerating human erythroid cells K562 apoptosis under PVP-coding Ag NPs exposure (Gao et al., 2017). Additionally, a recent study found that the inactivation of the X chromosome via lncRNA *Xist* and *Tsix* led to delayed differentiation of female mouse embryonic stem cells under low-dose Ag NPs exposure (Zhang et al., 2019). Overall, the study of lncRNA is still in the early stage of development, and more experiments are needed to determine which lncRNAs can be used as new biomarkers for toxicological responses to Ag NPs in the future. All results taken together, our study demonstrates that lncRNAs play an important role in *T. thermophila* to cope with Ag^+ and Ag NPs toxicity, including cell growth inhibition, cell membrane cation channel activation, and oxidoreductase activity promotion.

5. Conclusion

The physiological and lncRNA profiles obtained in this study provide deep insights into the toxic effect and epigenetic mechanisms in *T. thermophila* on exposure to Ag^+ and three types of Ag NPs. Results showed that these toxicants had substantial growth-inhibiting toxicity to *T. thermophila*, and the order of toxicity is Ag^+ > Ag-Cit10 > Ag-Cit80 > Ag-PVP80. All of these toxicants can generate a high level of ROS, which is responsible for the toxicity to *T. thermophila*, through lipid peroxidation and mitochondria dysfunction. As a defense mechanism against oxidative stress, *T. thermophila* activated an antioxidant response, such as increases of enzyme activities of GPx and Gr. Importantly, we identified 1250 differentially expressed lncRNAs and found these lncRNAs exhibited toxicant-specific expression patterns. Based on the lncRNA-mRNA co-expression networks, we showed that the lncRNA modules played an important regulatory role in *T. thermophila* to cope with the toxicity induced by Ag^+ and Ag NPs, including growth inhibition in all treatment groups, cell membrane cation channel activation in the Ag^+ treatment group, the promotion of oxidoreductase activity in Ag NP treatment groups.

CRediT authorship contribution statement

WZ and YP designed the experiments. YP performed the experiments. YP, WZ and SL analyzed data. YP, WZ and SL wrote the paper. WZ conceived the idea and supervised the research.

Declaration of competing interest

The authors declare that they have no conflict of interests.

Acknowledgments

WZ and YP designed the experiments. YP performed the experiments. YP, WZ and SL analyzed data. YP, WZ and SL wrote the paper. WZ conceived the idea and supervised the research. The authors wish to thank Prof. Miao Wei and Dr. Xiong Jie from the Institute of Hydrobiology, Chinese Academy of Sciences for providing the ciliated protozoa *T. thermophila* (strain SB210). This study was supported by the National Key Research and Development Program of China (2018YFC1406306 and 2018YFD0900702-3), the Fundamental Research Funds for the Central Universities (20720160115) and the National Marine Public Welfare Project of China (201505034).

Appendix A. Supplementary data

Supplementary data to this article can be found online at https://doi.org/10.1016/j.scitotenv.2020.144659.

References

Abdal Dayem, A., Hossain, M.K., Lee, S.B., Kim, K., Saha, S.K., Yang, G.M., Choi, H.Y., Cho, S.G., 2017. The role of reactive oxygen species (ROS) in the biological activities of metallic nanoparticles. Int. J. Mol. Sci. 18 (1), 120.

Abramenko, N.B., Demidova, T.B., Abkhalimov, E.V., Ershov, B.G., Krysanov, E.Y., Kustov, L.M., 2018. Ecotoxicity of different-shaped silver nanoparticles: case of zebrafish embryos. J. Hazard. Mater. 347, 89–94.

Akter, M., Sikder, M.T., Rahman, M.M., Ullah, A., Hossain, K.F.B., Banik, S., Hosokawa, T., Saito, T., Kurasaki, M., 2018. A systematic review on silver nanoparticles-induced cytotoxicity: physicochemical properties and perspectives. J. Adv. Res. 9, 1–16.

Al-Asadi, S., Malik, A., Bakiu, R., Santovito, G., Menz, I., Schuller, K., 2019. Characterization of the peroxiredoxin 1 subfamily from *Tetrahymena thermophila*. Cell. Mol. Life Sci. 76 (23), 4745–4768.

Bondarenko, O., Ivask, A., Kakinen, A., Kurvet, I., Kahru, A., 2013. Particle-cell contact enhances antibacterial activity of silver nanoparticles. PLoS One 8 (5), e64060.

Calderón-Jiménez, B., Johnson, M.E., Montoro Bustos, A.R., Murphy, K.E., Winchester, M.R., Vega Baudrit, J.R., 2017. Silver nanoparticles: technological advances, societal impacts, and metrological challenges. Front. Chem. 5, 6.

Chen, X., Sun, Y.Z., Guan, N.N., Qu, J., Huang, Z.A., Zhu, Z.X., Li, J.Q., 2019. Computational models for lncRNA function prediction and functional similarity calculation. Brief. Funct. Genomics 18 (1), 58–82.

Deponte, M., 2013. Glutathione catalysis and the reaction mechanisms of glutathione-dependent enzymes. Biochim. Biophys. Acta 1830 (5), 3217–3266.

Ferro, D., Bakiu, R., De Pittà, C., Boldrin, F., Cattalini, F., Pucciarelli, S., Miceli, C., Santovito, G., 2015. Cu, Zn superoxide dismutases from *Tetrahymena thermophila*: molecular evolution and gene expression of the first line of antioxidant defenses. Protist 166 (1), 131–145.

Finn, R.D., Coggill, P., Eberhardt, R.Y., Eddy, S.R., Mistry, J., Mitchell, A.L., Potter, S.C., Punta, M., Qureshi, M., Sangrador-Vegas, A., Salazar, G.A., Tate, J., Bateman, A., 2016. The Pfam protein families database: towards a more sustainable future. Nucleic Acids Res. 44 (D1), D279–D285.

Flores-Lopez, L.Z., Espinoza-Gomez, H., Somanathan, R., 2019. Silver nanoparticles: electron transfer, reactive oxygen species, oxidative stress, beneficial and toxicological effects. Mini review. J. Appl. Toxicol. 39 (1), 16–26.

Franchi, N., Ferro, D., Ballarin, L., Santovito, G., 2012. Transcription of genes involved in glutathione biosynthesis in the solitary tunicate *Ciona intestinalis* exposed to metals. Aquat. Toxicol. 114-115, 14–22.

Gao, M., Zhao, B., Chen, M., Liu, Y., Xu, M., Wang, Z., Liu, S., Zhang, C., 2017. Nrf-2-driven long noncoding RNA ODRUL contributes to modulating silver nanoparticle-induced effects on erythroid cells. Biomaterials 130, 14–27.

Gedda, M.R., Babele, P.K., Zahra, K., Madhukar, P., 2019. Epigenetic aspects of engineered nanomaterials: is the collateral damage inevitable? Front. Bioeng. Biotechnol. 7, 288.

Gloss, B.S., Dinger, M.E., 2016. The specificity of long noncoding RNA expression. Biochim. Biophys. Acta 1859 (1), 16–22.

Gomes, S.I.L., Roca, C.P., Scott-Fordsmand, J.J., Amorim, M.J.B., 2017. High-throughput transcriptomics reveals uniquely affected pathways: AgNPs, PVP-coated AgNPs and Ag NM300K case studies. Environ. Sci.: Nano 4, 929–937.

Hezroni, H., Koppstein, D., Schwartz, M.G., Avrutin, A., Bartel, D.P., Ulitsky, I., 2015. Principles of long noncoding RNA evolution derived from direct comparison of transcriptomes in 17 species. Cell Rep. 11 (7), 1110–1122.

Huynh, K.A., Chen, K.L., 2011. Aggregation kinetics of citrate and polyvinylpyrrolidone coated silver nanoparticles in monovalent and divalent electrolyte solutions. Environ. Sci. Technol. 45 (13), 5564–5571.

Ivask, A., Elbadawy, A., Kaweeteerawat, C., Boren, D., Fischer, H., Ji, Z., Chang, C.H., Liu, R., Tolaymat, T., Telesca, D., 2014a. Toxicity mechanisms in *Escherichia coli* vary for silver nanoparticles and differ from ionic silver. ACS Nano 8 (1), 374–386.

Ivask, A., Kurvet, I., Kasemets, K., Blinova, I., Aruoja, V., Suppi, S., Vija, H., Kakinen, A., Titma, T., Heinlaan, M., Visnapuu, M., Koller, D., Kisand, V., Kahru, A., 2014b. Size-dependent toxicity of silver nanoparticles to bacteria, yeast, algae, crustaceans and mammalian cells in vitro. PLoS One 9 (7), e102108.

Kim, D., Langmead, B., Salzberg, S.L., 2015. HISAT: a fast spliced aligner with low memory requirements. Nat. Methods 12 (4), 357–360.

Kong, L., Zhang, Y., Ye, Z.Q., Liu, X.Q., Zhao, S.Q., Wei, L., Gao, G., 2007. CPC: assess the protein-coding potential of transcripts using sequence features and support vector machine. Nucleic Acids Res. 35, W345–W349.

Langfelder, P., Horvath, S., 2008. WGCNA: an R package for weighted correlation network analysis. BMC Bioinformatics 9, 559.

Langmead, B., Salzberg, S.L., 2012. Fast gapped-read alignment with bowtie 2. Nat. Methods 9 (4), 357–359.

Li, B., Dewey, C.N., 2011. RSEM: accurate transcript quantification from RNA-Seq data with or without a reference genome. BMC Bioinformatics 12, 323.

Liu, S., Wang, Z., Chen, D., Zhang, B., Tian, R.R., Wu, J., Zhang, Y., Xu, K., Yang, L.M., Cheng, C., Ma, J., Lv, L., Zheng, Y.T., Hu, X., Zhang, Y., Wang, X., Li, J., 2017. Annotation and cluster analysis of spatiotemporal- and sex-related lncRNA expression in rhesus macaque brain. Genome Res. 27 (9), 1608–1620.

Lu, J., Zhang, S., Gao, S., Wang, P., Bond, P.L., Guo, J., 2020. New insights of the bacterial response to exposure of differently sized silver nanomaterials. Water Res. 169, 115205.

Luo, H., Bu, D., Sun, L., Fang, S., Liu, Z., Zhao, Y., 2017. Identification and function annotation of long intervening noncoding RNAs. Brief. Bioinform. 18 (5), 789–797.

Marchese, F.P., Raimondi, I., Huarte, M., 2017. The multidimensional mechanisms of long noncoding RNA function. Genome Biol. 18, 206.

Mortimer, M., Gogos, A., Bartolomé, N., Kahru, A., Bucheli, T.D., Slaveykova, V.I., 2014. Potential of hyperspectral imaging microscopy for semi-quantitative analysis of nanoparticle uptake by protozoa. Environ. Sci. Technol. 48 (15), 8760–8767.

Nallanthighal, S., Tierney, L., Cady, N.C., Murray, T.M., Chittur, S.V., Reliene, R., 2020. Surface coatings alter transcriptional responses to silver nanoparticles following oral exposure. NanoImpact 17, 100205.

Nayak, R.R., Kearns, M., Spielman, R.S., Cheung, V.G., 2009. Co-expression network based on natural variation in human gene expression reveals gene interactions and functions. Genome Res. 19 (11), 1953–1962.

Pan, Y., Zhang, W., Lin, S., 2018. Transcriptomic and microRNAomic profiling reveals molecular mechanisms to cope with silver nanoparticle exposure in the ciliate *Euplotes vannus*. Environ. Sci. Nano 5 (12), 2921–2935.

Pang, C., Brunelli, A., Zhu, C., Hristozov, D., Liu, Y., Semenzin, E., Wang, W., Tao, W., Liang, J., Marcomini, A., Chen, C., Zhao, B., 2016. Demonstrating approaches to chemically modify the surface of ag nanoparticles in order to influence their cytotoxicity and biodistribution after single dose acute intravenous administration. Nanotoxicology 10 (2), 129–139.

Pertea, M., Pertea, G.M., Antonescu, C.M., Chang, T.C., Mendell, J.T., Salzberg, S.L., 2015. StringTie enables improved reconstruction of a transcriptome from RNA-seq reads. Nat. Biotechnol. 33 (3), 290–295.

Piersanti, A., Juganson, K., Mozzicafreddo, M., Wei, W., Zhang, J., Zhao, K., Ballarini, P., Mortimer, M., Pucciarelli, S., Miao, W., Miceli, C., 2020. Transcriptomic responses to silver nanoparticles in the freshwater unicellular eukaryote *Tetrahymena thermophila*. Environ. Pollut. 115965.

Pillai, S., Behra, R., Nestler, H., Suter, M.J., Sigg, L., Schirmer, K., 2014. Linking toxicity and adaptive responses across the transcriptome, proteome, and phenotype of *Chlamydomonas reinhardtii* exposed to silver. Proc. Natl. Acad. Sci. U. S. A. 111 (9), 3490–3495.

Sekine, R., Moore, K.L., Matzke, M., Vallotton, P., Jiang, H., Hughes, G.M., Kirby, J.K., Donner, E., Grovenor, C.R.M., Svendsen, C., Lombi, E., 2017. Complementary imaging of silver nanoparticle interactions with green algae: dark-field microscopy, electron microscopy, and nanoscale secondary ion mass spectrometry. ACS Nano 11 (11), 10894–10902.

Silva, T., Pokhrel, L.R., Dubey, B., Tolaymat, T.M., Maier, K.J., Liu, X., 2014. Particle size, surface charge and concentration dependent ecotoxicity of three organo-coated silver nanoparticles: comparison between general linear model-predicted and observed toxicity. Sci. Total Environ. 468-469, 968–976.

Solioz, M., Odermatt, A., 1995. Copper and silver transport by CopB-ATPase in membrane vesicles of *Enterococcus hirae*. J. Biol. Chem. 270 (16), 9217–9221.

Sun, L., Luo, H., Bu, D., Zhao, G., Yu, K., Zhang, C., Liu, Y., Chen, R., Zhao, Y., 2013. Utilizing sequence intrinsic composition to classify protein-coding and long non-coding transcripts. Nucleic Acids Res. 41 (17), e166.

Tejamaya, M., Römer, I., Merrifield, R.C., Lead, J.R., 2012. Stability of citrate, PVP, and PEG coated silver nanoparticles in ecotoxicology media. Environ. Sci. Technol. 46, 7011–7017.

Tortella, G.R., Rubilar, O., Duran, N., Diez, M.C., Martinez, M., Parada, J., Seabra, A.B., 2020. Silver nanoparticles: toxicity in model organisms as an overview of its hazard for human health and the environment. J. Hazard. Mater. 390, 121974.

Ulm, L., Krivohlavek, A., Jurašin, D., Ljubojević, M., Šinko, G., Crnković, T., Žuntar, I., Šikić, S., Vinković Vrček, I., 2015. Response of biochemical biomarkers in the aquatic crustacean *Daphnia magna* exposed to silver nanoparticles. Environ. Sci. Pollut. Res. Int. 22 (24), 19990–19999.

Vance, M.E., Kuiken, T., Vejerano, E.P., McGinnis, S.P., Hochella Jr., M.F., Rejeski, D., Hull, M.S., 2015. Nanotechnology in the real world: redeveloping the nanomaterial consumer products inventory. Beilstein J. Nanotechnol. 6, 1769–1780.

Wang, L., Feng, Z., Wang, X., Wang, X., Zhang, X., 2010. DEGseq: an R package for identifying differentially expressed genes from RNA-seq data. Bioinformatics 26 (1), 136–138.

Wang, G., Jin, W., Qasim, A.M., Gao, A., Peng, X., Li, W., Feng, H., Chu, P.K., 2017. Antibacterial effects of titanium embedded with silver nanoparticles based on electron-transfer-induced reactive oxygen species. Biomaterials 124, 25–34.

Wu, Q., Zhou, X., Han, X., Zhuo, Y., Zhu, S., Zhao, Y., Wang, D., 2016. Genome-wide identification and functional analysis of long noncoding RNAs involved in the response to graphene oxide. Biomaterials 102, 277–291.

Xiu, Z.M., Zhang, Q.B., Puppala, H.L., Colvin, V.L., Alvarez, P.J., 2012. Negligible particle-specific antibacterial activity of silver nanoparticles. Nano Lett. 12 (8), 4271–4275.

Yang, X., Gondikas, A.P., Marinakos, S.M., Auffan, M., Liu, J., Hsu-Kim, H., Meyer, J.N., 2012. Mechanism of silver nanoparticle toxicity is dependent on dissolved silver and surface coating in *Caenorhabditis elegans*. Environ. Sci. Technol. 46 (2), 1119–1127.

Yang, Y., Xu, S., Xu, G., Liu, R., Xu, A., Chen, S., Wu, L., 2019. Effects of ionic strength on physicochemical properties and toxicity of silver nanoparticles. Sci. Total Environ. 647, 1088–1096.

Yu, J., Loh, X.J., Luo, Y., Ge, S., Fan, X., Ruan, J., 2020. Insights into the epigenetic effects of nanomaterials on cells. Biomater. Sci. 8 (3), 763–775.

Zhang, J., Chen, Y., Gao, M., Wang, Z., Liu, R., Xia, T., Liu, S., 2019. Silver nanoparticles compromise female embryonic stem cell differentiation through disturbing X chromosome inactivation. ACS Nano 13 (2), 2050–2061.